https://doi.org/10.5607/en.2018.27.5.397
Exp Neurobiol. 2018 Oct;27(5):397-407.
pISSN 1226-2560 • eISSN 2093-8144

Original Article

Experimental Neurobiology

Check for updates

Differential Expression of Ca^{2+}-buffering Protein Calretinin in Cochlear Afferent Fibers: A Possible Link to Vulnerability to Traumatic Noise

Kushal Sharma[1†], Young-Woo Seo[2†] and Eunyoung Yi[1*]

[1]College of Pharmacy and Natural Medicine Research Institute, Mokpo National University, Muan 58554,
[2]Korea Basic Science Institute Gwangju Center, Gwangju 61186, Korea

The synaptic contacts of cochlear afferent fibers (CAFs) with inner hair cells (IHCs) are spatially segregated according to their firing properties. CAFs also exhibit spatially segregated vulnerabilities to noise. The CAF fibers contacting the modiolar side of IHCs tend to be more vulnerable. Noise vulnerability is thought to be due to the absence of neuroprotective mechanisms in the modiolar side contacting CAFs. In this study, we investigated whether the expression of neuroprotective Ca^{2+}-buffering proteins is spatially segregated in CAFs. The expression patterns of calretinin, parvalbumin, and calbindin were examined in rat CAFs using immunolabeling. Calretinin-rich fibers, which made up ~50% of the neurofilament (NF)-positive fibers, took the pillar side course and contacted all IHC sides. NF-positive and calretinin-poor fibers took the modiolar side pathway and contacted the modiolar side of IHCs. Both fiber categories juxtaposed the C-terminal binding protein 2 (CtBP2) puncta and were contacted by synaptophysin puncta. These results indicated that the calretinin-poor fibers, like the calretinin-rich ones, were afferent fibers and probably formed functional efferent synapses. However, the other Ca^{2+}-buffering proteins did not exhibit CAF subgroup specificity. Most CAFs near IHCs were parvalbumin-positive. Only the pillar-side half of parvalbumin-positive fibers coexpressed calretinin. Calbindin was not detected in any nerve fibers near IHCs. Taken together, of the Ca^{2+}-buffering proteins examined, only calretinin exhibited spatial segregation at IHC-CAF synapses. The absence of calretinin in modiolar-side CAFs might be related to the noise vulnerability of the fibers.

Key words: cochlear afferent fiber, calretinin, inner hair cell synapse, Ca^{2+}-buffering protein

INTRODUCTION

Cochlear afferent fibers (CAFs) send auditory information from sensory hair cells to the brain. Although they comprise only a quarter of the cochlear hair cell population, inner hair cells (IHCs) receive over 90% of CAF innervations [1]. Each IHC is contacted by 10~30 CAFs that have diverse firing properties [2, 3], and their synaptic junctions are organized according to their firing properties. Fibers with low spontaneous rates (SRs), high thresholds, and large dynamic ranges (low-SR fibers) mainly synapse on the modiolar side of IHCs, while fibers with high SRs, low thresholds, and narrow dynamic ranges (high-SR fibers) preferentially contact the pillar side [4-6]. Various pre- and post-synaptic characteristics, such as ribbon size, Ca^{2+}-channel cluster, α-amino-3-hydroxy-5-methyl-4-isoxazolepropionic acid (AMPA) receptor patch size,

Received September 11, 2018, Revised September 28, 2018,
Accepted October 2, 2018

*To whom correspondence should be addressed.
TEL: 82-61-450-2683, FAX: 82-61-450-2689
e-mail: eunyoungyi@mokpo.ac.kr
†These authors contributed equally.

and fiber thickness [7, 8], differ between the pillar and modiolar sides. However, these findings cannot explain why modiolar-side contacting fibers seem more vulnerable to noise [6]. Considering their resting firing rate, sound threshold, dynamic range, and maximum firing rate, the amount of glutamate released at low-SR-fiber synapses does not appear greater than that at high-SR-fiber synapses. Analyses of electron micrographs of IHCs have suggested that the higher vesicle number in modiolar synaptic ribbons is due to less glutamate release [9] and that the higher noise vulnerability of modiolar CAFs is due to post-glutamate release events. Additional factors proposed to contribute to higher noise vulnerability are poor glutamate removal from the synaptic cleft and/or an absence of neuroprotective mechanisms [10]. Calretinin, a Ca^{2+}-buffering protein with neuroprotective mechanisms against glutamate-induced excitotoxicity [11], was poorly expressed in nerve fibers contacting the IHC modiolar side [12]. Thus, we hypothesized that the differential expression patterns of Ca^{2+}-buffering proteins are related to the relative noise vulnerability of CAFs. Using immunolabeling and confocal microscopy we investigated whether Ca^{2+}-buffering proteins, including calretinin, exhibit spatially segregated expression patterns in IHC-CAF synapses.

MATERIALS AND METHODS

Animals

All animal procedures were approved by the Institutional Animal Care and Use Committees of Mokpo National University (MNU-IACUC-2017-001). Sprague-Dawley rats were euthanized by sevoflurane overdoses and then decapitated.

Immunohistochemistry

Cochleae were dissected from the animals, perfused through either the oval or round windows with ice-cold 4% paraformaldehyde (pH 7.4), and then fixed in 4% paraformaldehyde (1 h, 4°C). The cochlear tissues were excised, immersed in blocking buffer (phosphate-buffered saline containing 5% donkey or goat serum and 0.25% Triton-X-100) for 1 h at room temperature, and then incubated with primary antibodies (overnight, 4°C). The next day, the tissues were washed 3 times with blocking buffer and then incubated with fluorescent-tagged secondary antibodies (1 h, room temperature). After removing the unreacted secondary antibodies, the tissue was mounted on slides using FluorSave™ mounting medium (cat. #345789, EMD Millipore Corporation, Billerica, MA, USA). Images of the tissue were obtained using a Confocal Laser Scanning Microscope (Leica TCS SP5/AOBS/Tandem [Leica Mikrosysteme Vertrieb GmbH, Wetzlar, Germany] at the Korea Basic Science Institute Gwangju Center or Zeiss LSM 710 [Carl ZEISS AG, Oberkochen, Germany] at Mokpo National University). Three-dimensional z-stack images were obtained with 0.3~0.99 μm z-step intervals. Image analyses were conducted using image viewing software provided by the microscope manufacturers (ZEISS ZEN [Carl ZEISS AG] or Leica LAS AF Lite [Leica Mikrosysteme Vertrieb GmbH]) and Imaris (Bitplane AG, Zurich, Switzerland). The tracing of CAFs began from the nerve terminals where they contact the either side of IHC. After marking the terminals, we traced each fibers retrogradely as far as possible, by comparing adjacent single confocal slices, 3D reconstruction images and XZ and ZY projection views. Then, Imaris tracing was attempted in part of these manually-traced fibers. The Surface and FilamentTracer modules of Imaris were used to trace and visualize the nerve fibers. The processed nerve fibers were displayed as curved cylinders with constant widths.

To compare calretinin-content of CAFs we analyzed the NKA- and calretinin-immunofluorescence in ROIs placed on the boutons on either side of the IHC. Because calretinin is also present in the IHC the calretinin-immunofluorescence in ROIs on boutons is often confounded by the signals from the IHC. The calretinin-signal from IHC was estimated from control ROI, placed immediately adjacent to each ROI on bouton. The calretinin-immunofluorescence in each ROI on bouton was then calculated by subtracting control ROI signal from the raw data on bouton.

No labeling was observed when the primary antibodies were omitted. The following primary antibodies were used: anti-calretinin (MAB1568, 1:500; AB5054, 1:500; EMD Millipore Corporation), anti-parvalbumin (PVG-213, 1:500~1000; Swant, Marly, Switzerland), anti-calbindin (CB-38a, 1:500; Swant), anti-neurofilament heavy polypeptide (NF; AB5539, 1:1,000; EMD Millipore Corporation), anti-Na^+, K^+-ATPase α3 (NKA; MA3-915, 1:500 [Thermo Fisher Scientific Inc., Waltham, MA, USA]; sc-16052, 1:500 [Santa Cruz Biotechnology, Inc., Dallas, TX, USA]), anti-C-terminal binding protein 2 (CtBP2; cat. #612044, 1:500; BD Biosciences, San Jose, CA, USA), anti-myosin 7a (cat. #25-6790, 1:500; Proteus BioSciences Inc., Ramona, CA, USA), and anti-synaptophysin (MAB5258, 1:500; EMD Millipore Corporation). The Alexa Fluor 647 (AP194SA6, 1:1000)-conjugated donkey anti-chicken secondary antibody was from the EMD Millipore Corporation. All other secondary antibodies (1:1000) were from Thermo Fisher Scientific Inc.

RESULTS

Segregated dendritic pathways of calretinin-rich and -poor nerve fibers

A recent study reported that calretinin-poor and β-3 tubulin-

https://doi.org/10.5607/en.2018.27.5.397

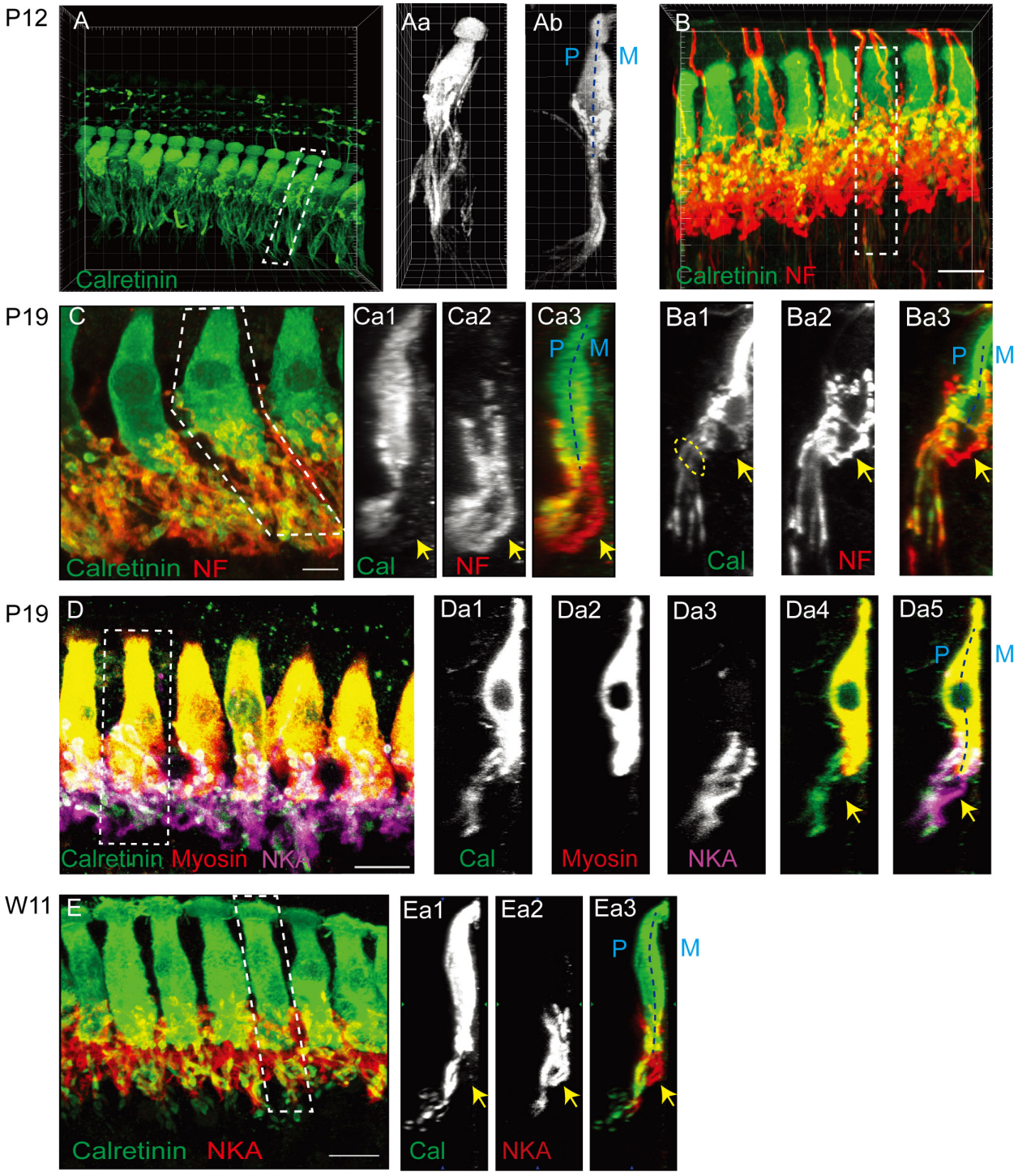

Fig. 1. Differential trajectories of the cochlear afferent fibers (CAFs) in the organ of Corti. (A) A three-dimensional (3D) reconstructed image of the organ of Corti immunolabeled with anti-calretinin in a P12 rat. (Aa~Ab) XY and ZY projection views of the marked area in A. (B) 3D-reconstructed images of an organ of Corti in a P11 rat that is double-immunolabeled with anti-calretinin (green) and anti-neurofilament (NF; red). (Ba1~Ba3) ZY section views of the marked area in B. An approximate location of habenular perforata is marked with dotted oval. (C) A 3D reconstructed image of an organ of Corti from a P19 rat that was double-immunolabeled with anti-calretinin (green) and anti-NF (red). (Ca1~Ca3) ZY projection views of the marked area in C. (D) A 3D reconstructed image of an organ of Corti from a P19 rat that was triple-immunolabeled with anti-calretinin (green), anti-myosin (red) and anti-NKA (magenta). (Da1~Da5) ZY section views of the marked area in D. (E) A 3D reconstructed image of an organ of Corti from a 11-week-old rat (W11) that was double-immunolabeled with anti-calretinin (green) and anti- Na, K-ATPase alpha 3 (NKA; red). (Ea1~Ea3) ZY projection view of the marked area in E. At all ages examined, calretinin-rich and calretinin-poor fibers (arrow) exhibit segregated courses. The pillar (P) and modiolar side (M) of IHC is marked with dotted lines (Ab, Ba3, Ca3, Da5, and Ea3).

positive nerve fibers contact the modiolar side of IHCs [12]. Thus, of the Ca^{2+}-buffering proteins, we first investigated calretinin and analyzed its expression patterns in IHC-CAF synapses. As previously reported [13-15], calretinin immunoreactivity was found in the cytosol of hair cells and CAFs (Fig. 1). The strongest calretinin signals were observed in bouton terminals. Calretinin-rich terminals contacted all IHC sides (Fig. 1Ab). A well-known CAF marker, NF, exhibited a similar pattern. NF-positive fibers terminated on all IHC sides (Fig. 1B). However, further examination revealed striking differences between calretinin- and NF-positive fibers.

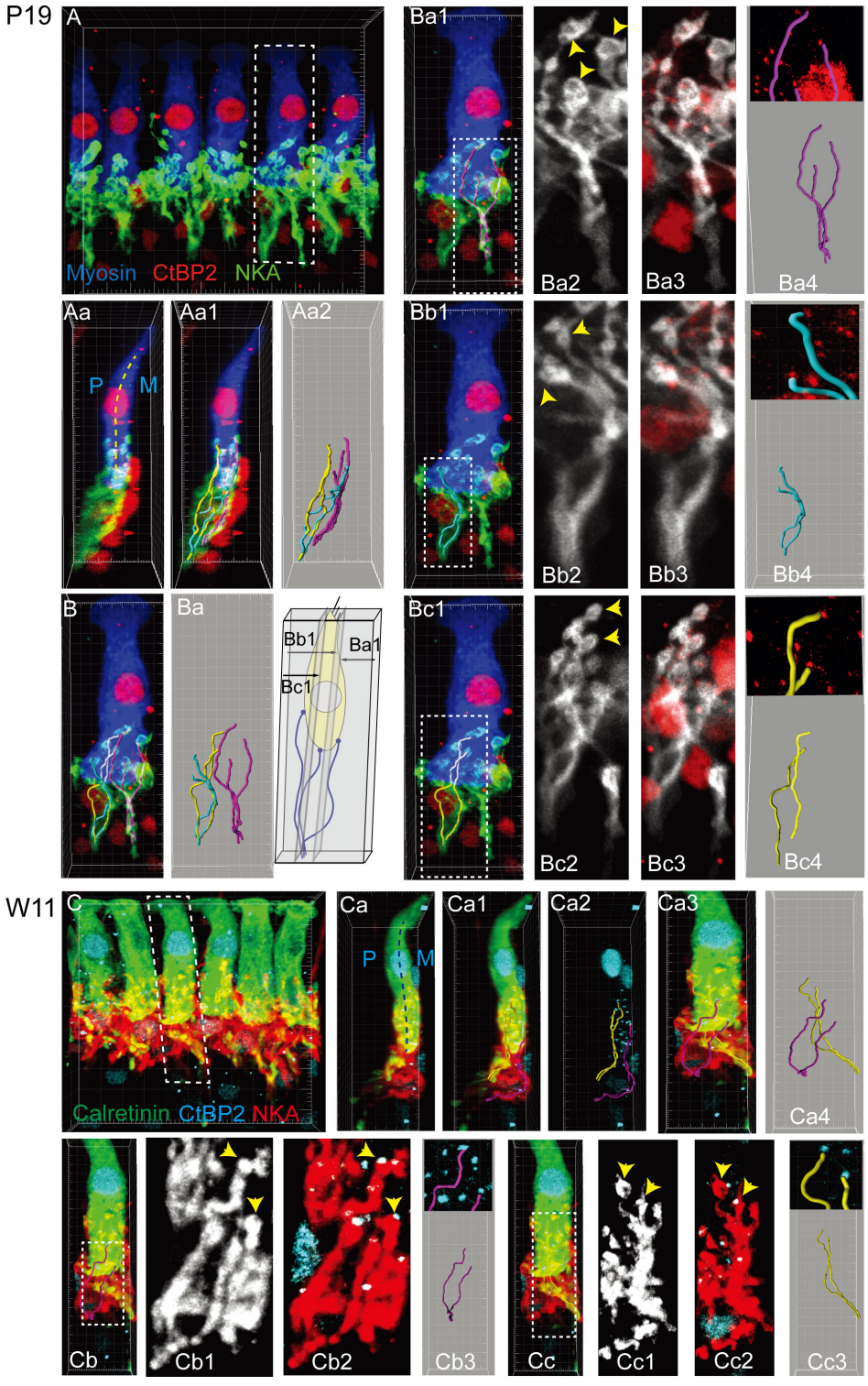

Fig. 2. Both calretinin-rich and -poor nerve fibers juxtapose synaptic ribbons. (A) A 3D reconstructed image of an organ of Corti of a P19 rat that is triple-immunolabeled with anti-myosin VIIa (blue), anti-C-terminal binding protein 2 (CtBP2; red), and anti-NKA (green). A 3D image of a single IHC and its associated nerve fibers (marked area) was extracted and processed for further analysis in Aa~Bc4. (Aa) ZY projection view. (B) XY projection view. (Ba1~Bc4) XY projection views from partial Z stacks, as described in diagram. (Ba2~Ba3) XY projection views of the marked area in Ba1. (Bb2~Bb3) XY projection views of the marked area in Bb1. (Bc2~Bc3) XY projection views of the marked area in Bc1. The trajectories of 7 exemplary NKA-positive nerve fibers were traced and displayed in curved cylinders according to their courses after passing the habenula perforata. Magenta: fibers with a modiolar-side course and terminating on the modiolar side of the IHCs. Cyan: fibers with a pillar-side course and terminating on the modiolar side of the IHCs. Yellow: fibers with a pillar-side course and terminating on the pillar side of the IHCs. (C) A 3D reconstructed image of an organ of Corti of a 11-week-old rat that is triple-immunolabeled with anti-calretinin (green), anti-CtBP2 (cyan), and anti-NKA (red). A 3D image of a single IHC and its associated nerve fibers (marked area) was extracted and processed for further analysis in Ca~Cc3. (Ca~Ca2) ZY projection view. (Ca3) XY projection view. (Cb1~Cb2) XY projection views of the marked area in Cb. (Cc1~Cc2) XY projection views of the marked area in Cc. Magenta: calretinin-poor fibers terminating on the modiolar side of the IHCs. Yellow: calretinin-rich fibers terminating on the pillar side of the IHCs. Regardless of their courses, all traced fibers juxtaposed CtBP2 puncta (insets). The pillar (P) and modiolar side (M) of IHC is marked with dotted lines (Aa and Ca).

https://doi.org/10.5607/en.2018.27.5.397

Only 52% of the identifiable NF-positive fibers were calretinin-rich (135/259 NF-positive fibers, P11-12, 3 preparations, 26 IHC regions), and significant portions of NF-positive fibers did not exhibit any calretinin immunoreactivity (Fig. 1Ba1~Ba3). Moreover, the calretinin-poor fibers had a trajectory that was segregated from the trajectories of the rest of the fibers. After crossing the habenula perforata (Fig. 1Ba1, dotted oval), the calretinin-rich fibers (Fig. 1Ba1, 1Ba3) tended to project straight toward the basal pole of the IHCs and then spread to all IHC sides. In contrast, calretinin-poor fibers (Fig. 1Ba2~Bb3, arrow) exhibited a winding course around the inner support cells and predominantly terminated on the modiolar side of the IHCs.

To determine whether this segregation was a temporary phenomenon during development or persisted until adulthood, cochlear tissues from older animals (P19 and 11-week-old (W11)) were examined. In P19 cochlea, NF-positive fibers also exhibited segregated trajectories depending on their calretinin immunoreactivity (Fig. 1C). Calretinin-rich fibers took a more pillar side

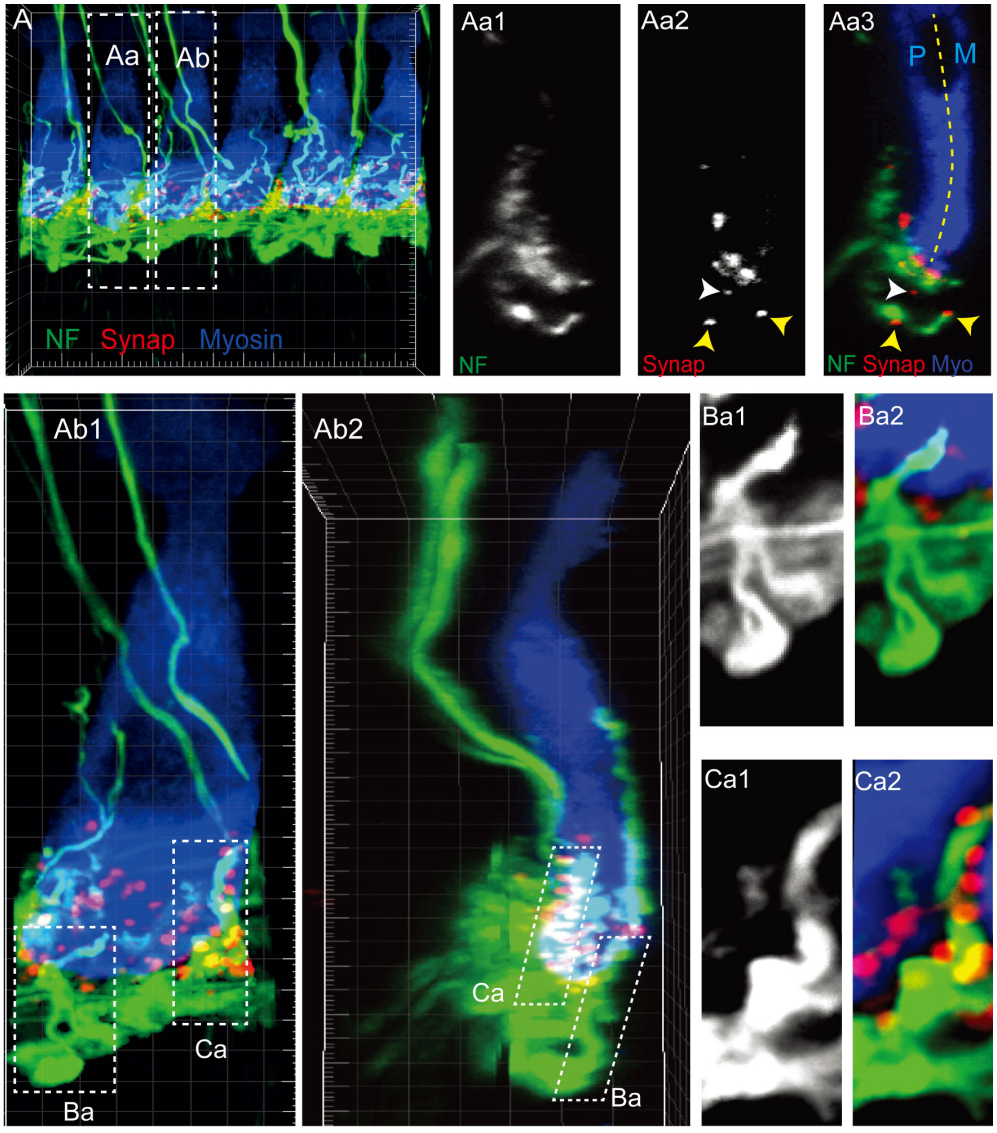

Fig. 3. Efferent nerve terminals contact CAFs regardless of their fiber courses. (A) A 3D-reconstructed image of an organ of Corti of a P16 rat triple-immunolabeled with anti-myosin VIIa (blue, myosin), anti-synaptophysin (red, Synap), and anti-NF (green). 3D images of a single IHC and its associated nerve fibers (marked areas with dotted rectangles) were extracted and processed for further analysis in Aa1-Aa3 and Ab1~Ca2. (Aa1~Aa3) ZY section view. NF-positive fibers with segregated routes are both contacted by synaptophysin puncta (yellow and white arrowheads). (Ab1~Ab2) XY and ZY projection views. (Ba1~Ba2) fibers with a modiolar-side course and terminating on the modiolar side of the IHCs. (Ca1~Ca2) fibers with a pillar-side course and terminating on the pillar side of the IHCs. Regardless of their courses, all traced fibers contacted synaptophysin puncta. The pillar (P) and modiolar side (M) of IHC is marked with dotted line (Aa3).

pathway and contacted all IHC sides (Fig. 1Ca1, 1Ca3), while calretinin-poor fibers showed a more modiolar course and contacted IHCs on the modiolar side (Fig. 1Ca2~Da3, arrow). Immunolabeling with another CAF marker, NKA [16], was essentially identical to the anti-NF immunolabeling (Fig. 1D, 1E, and 2). To avoid mistakenly following MOC efferent fibers [16], we often started tracing from the NKA-positive bouton terminals and tracked toward the habenula perforata. NKA-positive fibers of P19 and W11 cochleae also exhibited segregated courses depending on their calretinin content (Fig. 1Da1~Da5, 1Ea1~Ea3, arrow). These results suggested that the calretinin-dependent differential projections of CAFs were determined in early development and maintained until adulthood.

Afferent and efferent synaptic contacts of calretinin-rich and -poor nerve fibers

We next investigated whether the calretinin-poor fibers were functional CAFs by co-labeling the fibers with the synaptic ribbon marker CtBP2. NKA-positive fibers, regardless of their trajectories, terminated near CtBP2 puncta (Fig. 2Ba4, 2Bb4, 2Bc4, 2Cb3, 2Cc3, insets). In addition, both calretinin-rich and -poor nerve terminals juxtaposed CtBP2-puncta (Fig. 2Cb3, 2Cc3, insets). These findings indicated that calretinin-poor fibers probably conveyed afferent signals.

We then investigated whether the efferent synaptic innervation differed between fibers with different trajectories. Co-labeling with synaptophysin, an efferent marker, indicated that both groups of fibers were contacted by synaptophysin puncta (Fig. 3). No identifiable differences were observed in the synaptophysin labeling among them.

Ca^{2+}-buffering proteins in CAFs

Cochlear afferent neurons contain multiple Ca^{2+}-buffering proteins, such as calretinin, parvalbumin, and calbindin [17-20]. However, it is unknown whether Ca^{2+}-buffering proteins other than calretinin exhibit any specificity among CAF subgroups. Here, we compared the expression of calretinin, parvalbumin, and calbindin in SGNs. All 3 proteins were found in NF- or NKA-positive SGNs (Fig. 4A, B). Calretinin was found in 50% of the NF- or NKA-positive SGNs (123/245 SGNs, 5 preparations). These results were consistent with the results for the fibers near the IHCs. Similarly, a recent study reported that ~50% of rat SGNs were calretinin-positive [21]. In contrast, parvalbumin and calbindin were present in most SGNs (91%, 166/183 NF- or NKA-positive

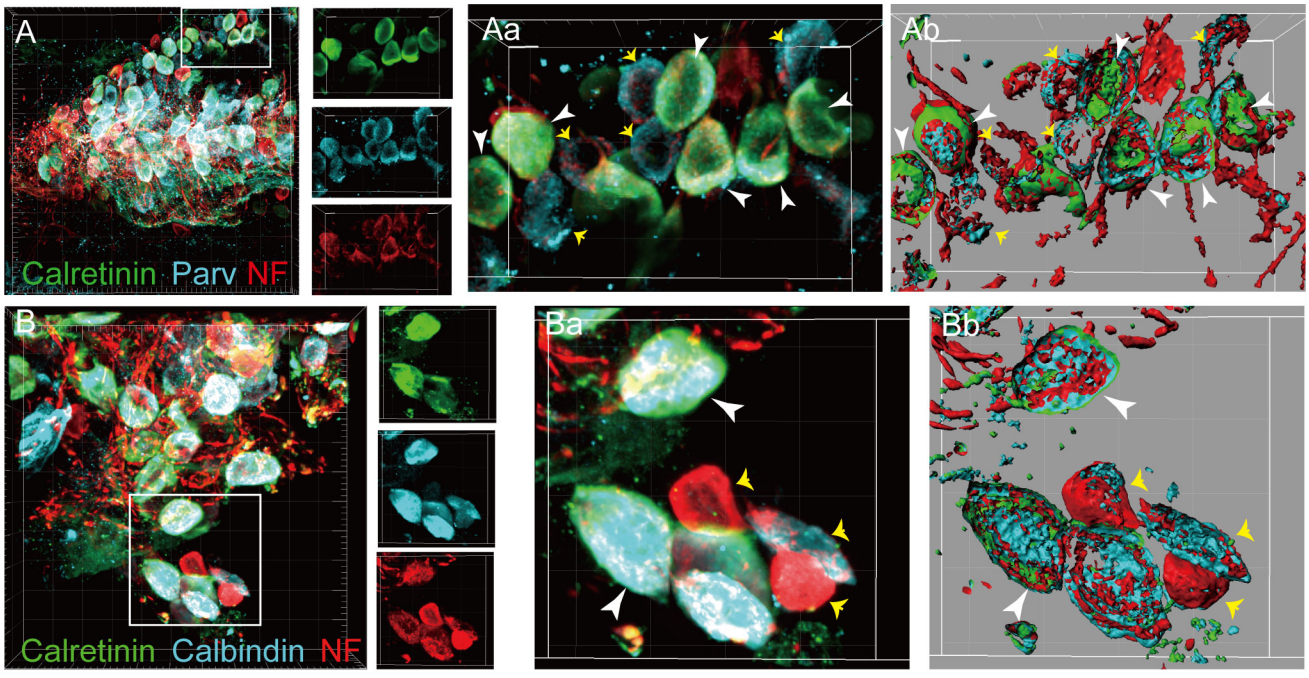

Fig. 4. The patterns of expression of calretinin, parvalbumin, and calbindin in SGNs. (A) SGNs triple-immunolabeled for anti-calretinin (green), anti-parvalbumin (Parv; cyan), and anti-NF (red). SGNs containing different sets of Ca^{2+}-buffering proteins are distinguishable at high magnification (Aa) and in surface object images (Ab). White arrowheads: SGNs with calretinin, parvalbumin, and NF. Yellow arrows: SGNs with parvalbumin and NF. (B) SGNs triple-immunolabeled for anti-calretinin (green), anti-calbindin (cyan), and anti-NF (red). SGNs containing different sets of Ca^{2+}-buffering proteins are distinguishable at high magnification (Ba) and in surface object images (Bb). White arrowheads: SGNs with calretinin, calbindin, and NF. Yellow arrows: SGNs with calbindin and NF.

https://doi.org/10.5607/en.2018.27.5.397

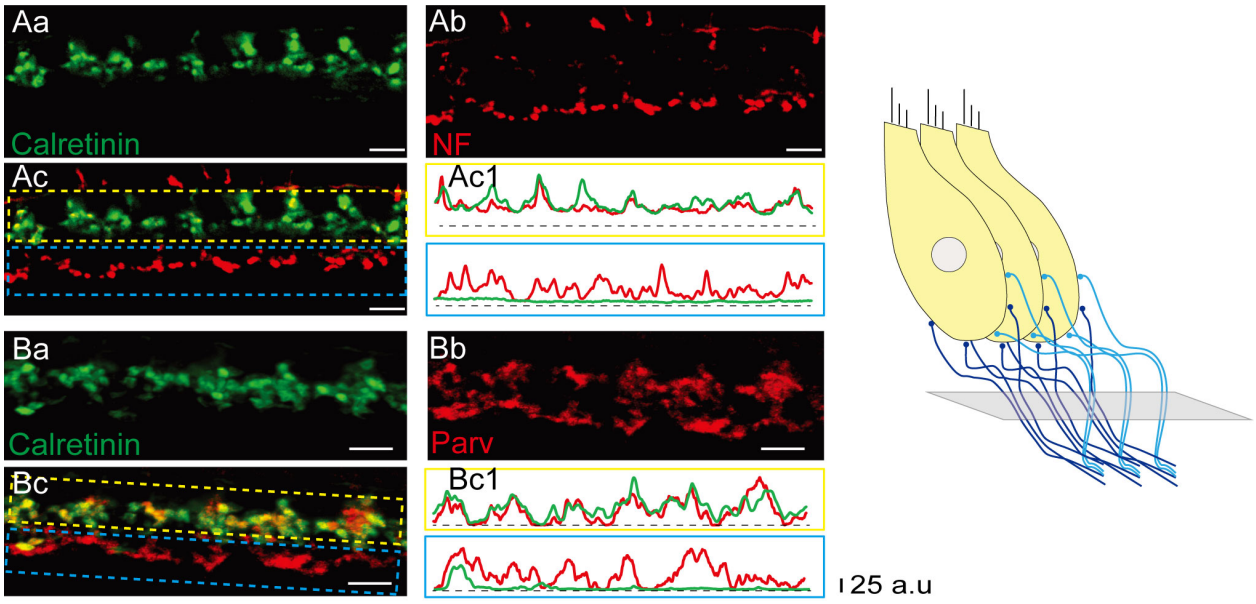

Fig. 5. The expression patterns of calretinin and parvalbumin in CAFs. (Aa~Ac) Cross-sectional view of CAFs double-immunolabeled for anti-calretinin and anti-NF. (Ac1) Plot of the immunofluorescence intensity in the areas marked by the yellow and cyan rectangles in Ac. (Ba~Bc) Cross-sectional view of CAFs double-immunolabeled with anti-calretinin and anti-parvalbumin. (Bc1) Plot of the immunofluorescence intensity in the areas marked by the yellow and cyan rectangles in Bc. The approximate cross-sectional position of the Aa~Ac and Ba-Bc images are described in the diagram on the right. Calretinin is found mostly in fibers on the pillar side, while parvalbumin is present in most fibers.

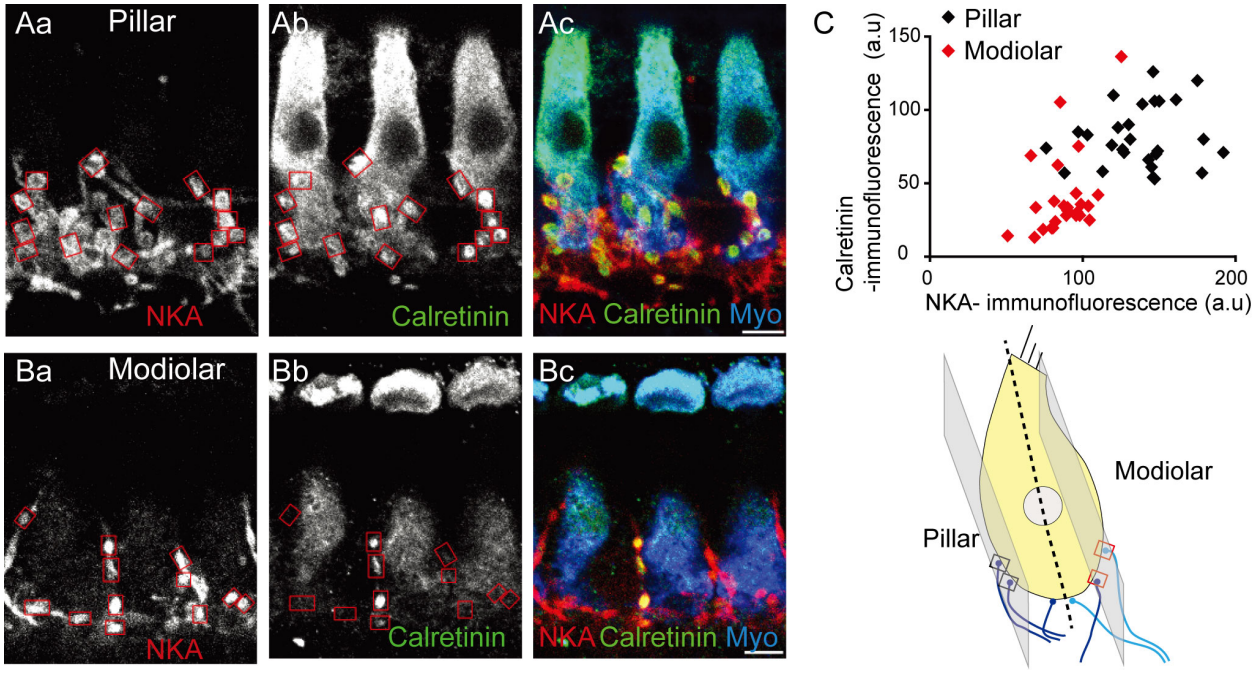

Fig. 6. The expression pattern of calretinin in the bouton endings of CAFs. (Aa~Bc) Single confocal slice images representing the pillar- (Aa~Ac) and modiolar- (Ba~Bc) sides of the IHC (red, NKA; green, calretinin; Blue, myosin). (C) Scatter plot of the NKA- and calretinin-immunofluorescence intensity in ROIs (red rectangles in Aa~Ab, Ba~Bb) placed on the boutons on either side of the IHC. The approximate positions of the ROIs are described in the diagram below. The ROIs on the pillar-side (black) boutons exhibited higher calretinin-immunofluorescence than the ROIs on the modiolar-side ones (red). In addition, the pillar-side boutons appear slightly bigger and exhibit higher NKA-immunofluorescence than the modiolar-side ones.

SGNs, 4 preparations; 95%, 106/112 SGNs, 2 preparations). Not surprisingly, most calretinin-rich neurons were also parvalbumin- or calbindin-positive (Fig. 4Aa~Ab, 4Ba~Bb, white arrows), while a significant portion of the parvalbumin- or calbindin-positive neurons were calretinin-poor (Fig. 4Aa~Ab, 4Ba~Bb, yellow arrows).

We then investigated whether the trajectories of calretinin-rich neurons differed from those of parvalbumin- or calbindin-positive neurons. Cross-sectional views of tissue from about halfway between the habenula perforata and the IHC base (Fig. 5 diagram) revealed calretinin immunoreactivity in the fibers taking pillar side route (Fig. 5Aa~Ac, 5Ac1, yellow box) but not in those following the more modiolar path (Fig. 5Aa~Ac, 5Ac1, cyan box). We also analyzed NKA- and calretinin-immunofluorescence in ROIs placed on the boutons on either side of the IHC (Fig. 6Aa~Ac, the pillar-side of the IHC; 6Ba~Bc, the modiolar-side of the IHC). The scatter plot in Fig. 6C indicated that the ROIs on the pillar-side (black) boutons exhibited higher calretinin-immunofluorescence than the ROIs on the modiolar-side ones (red), further confirming the calretinin-dependent segregated paths of CAFs. In contrast, parvalbumin immunoreactivity was detected in fibers of both paths (Fig. 5Ba~Bc, 5Bc1). Unlike parvalbumin and calretinin, calbindin was not detected in any nerve fibers near the IHCs. Yet, calbindin-positive CAFs have been detected in some previous studies [22, 23]. We presumed that the inconsistency might be due to the different experimental conditions but did not pursue further. Taken together, among the various Ca^{2+}-buffering proteins tested, calretinin was the only marker that distinguished the CAFs exhibiting segregated courses.

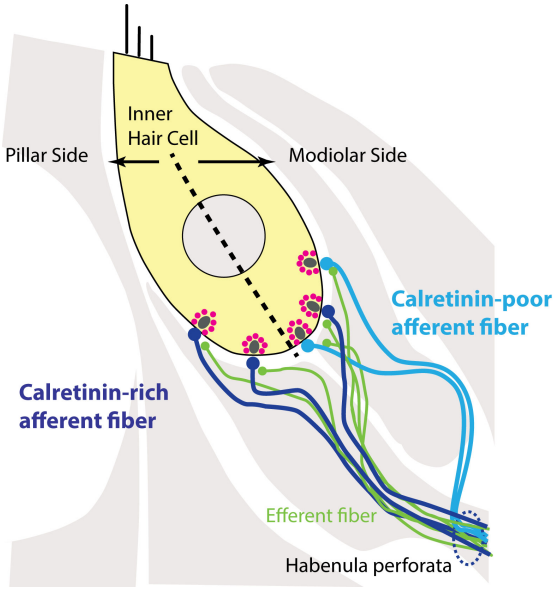

Fig. 7. Cochlear afferent fibers with differential calretinin content and dendritic trajectories. Calretinin-rich fibers contact all IHC sides, while calretinin-poor fibers predominantly synapse on the modiolar side of IHCs. Both groups of fibers make afferent and efferent synapses.

DISCUSSION

We showed that, at all ages examined, CAFs exhibited segregated dendritic trajectories: calretinin-rich fibers exhibited a pillar-side route and synapsed on all IHC sides, while the remaining calretinin-poor fibers showed a modiolar-side course and predominantly contacted the modiolar side of IHCs (Fig. 7). Similarly segregated CAF dendritic trajectories have been reported in previous reports investigating perinatal mouse cochlea [24, 25] and rat cochlea [12, 26], which suggests that the phenomenon is not limited to rats in certain developmental periods.

The neurite growth of CAFs is guided by multiple factors, including neurotrophic factors, extracellular matrix proteins, and cell adhesion molecules [24, 27-31]. Molecular cues from hair cells and support cells in the organ of Corti appear to provide important guidance for initial pathfinding. Considering the segregated dendritic trajectories in the perinatal cochleae [25, 27], the determining factor(s) must function earlier. During embryonic development, CAFs reach the organ of Corti (E14.5 in mouse) before the first hair cell differentiation (E16.5) [29], which suggests that the initial dendritic segregation could have been arranged even before hair cell differentiation. Alternatively, the segregated trajectories might be organized during the refinement period. IHC-CAF synapses are initially diffuse, with each fiber often making multiple contacts with more than one IHCs. Then, during the remaining embryonic days and first postnatal week, IHC-CAF synapses undergo significant pruning and reorganization, which leaves a single dendritic contact for each fiber [32]. Molecular cues, such as cadherins [31] and ephrins/Ephs [27], are highly expressed in the perinatal organ of Corti, and they provide guidance during the neurite growth and refinement period. It would be interesting to investigate whether these molecular cues are also involved in segregating the dendritic trajectories.

Low- and mid-SR fibers tend to contact IHCs on the modiolar side, whereas high-SR fibers more likely contact them on the pillar side [4, 5]. Our results demonstrated that calretinin-poor fibers predominantly contacted the IHCs on the modiolar side. Then, are the calretinin-poor fibers low-SR fibers? At least until ~P14, the presence of calretinin and the SRs of CAFs do not appear to be directly correlated. Previous findings from excised postnatal cochleae indicated that the diversity of SRs developed gradually during developmental period and high-SR fibers emerged from the third postnatal week [15, 33]. Most fibers until ~P14, although many of them are calretinin-positive [13, 16, 21], have low- or

https://doi.org/10.5607/en.2018.27.5.397

mid-SRs [15, 33]. However, the maturation and diversification of IHC-CAF synapses continue until ~4 weeks after birth [33, 34]. The firing properties of CAFs are thought to be influenced by multiple pre- and postsynaptic elements of the IHC-CAF synapse. The size of presynaptic ribbon, the size of the postsynaptic AMPA receptor patch, the efficiency of the Ca^{2+} influx–exocytosis coupling, the number and voltage-dependence of Ca^{2+} channel have been suggested to be the important contributing factors [7, 35-37]. Interestingly, the efficiency of the Ca^{2+} influx–exocytosis coupling improved dramatically during the third postnatal week [35]. In addition, the amplitude and voltage-dependence of Ca^{2+} influx among the different presynaptic ribbons of IHCs became much more diverse after ~P14 [36, 37]. Thus, the evidence to date has not excluded the possibility that neonatal calretinin-rich fibers later become high-SR fibers while calretinin-poor fibers remain low-SR fibers.

Another interesting issue was if the absence of calretinin in CAFs was related to vulnerability to noise. In animal models, loud sounds cause the swelling and degeneration of CAF terminals [18, 38]. Similar CAF terminal swelling could be evoked by exogenous glutamate agonists and alleviated by glutamate antagonists [39], thus suggesting that noise-induced swelling results from glutamate excitotoxicity. The differential distribution of certain neuroprotective mechanisms in IHC-CAF synapses has been suggested to contribute to the differences in vulnerability. For example, the glutamate eliminating transporter GLAST seems more sparsely distributed in the modiolar-side support cells than in the pillar-side cells [10]. Modiolar-side fibers contained less mitochondria, which made them less efficient in maintaining proper ion gradients [6]. In this study, we demonstrated a differential distribution of the Ca^{2+}-buffering protein calretinin in CAFs. Calretinin, parvalbumin, and calbindin are EF-hand Ca^{2+} buffers with different Ca^{2+}-binding properties [40, 41]. Parvalbumin acts as a simple Ca^{2+} buffer. Calbindin is a fast-onset buffer and can affect the early rising phase of the Ca^{2+} transient. Calretinin is a slow-onset buffer with high cooperativity. Such high cooperativity might be more advantageous for preventing Ca^{2+} overload-associated toxicity. In a transfected neuroblastoma-retina hybrid cell system, calretinin appears to attenuate glutamate-induced toxicity [11], which supports the potential neuroprotective role of calretinin. Similarly, calretinin-positive cortical neurons were more resistant to Ca^{2+}-overloading agent or glutamate receptor agonists than calretinin-negative neurons grown in the same culture dish [42]. Calretinin-rich gerbil mossy cells in dentate gyrus survived excitotoxic insult better than calretinin-poor rat mossy cells [43]. An examination on calretinin-/- mice also implicated a potential role of calretinin on neuronal survival. The dentate gyrus stem cell niche of calretinin-/- mice exhibited an early loss of proliferative capacity and an impaired hippocampal neurogenesis, suggesting that calretinin provide a maintenance signal for neuronal survival/differentiation [44].

Calretinin is expressed in many auditory neurons, and its expression level can vary depending on auditory experiences. In deafferentiated animals, neurons in the ipsilateral cochlear nuclei exhibit decreased calretinin staining [45-47]. In contrast, rats exposed to a moderate-level sound exhibit increased calretinin staining in the cochlear nuclei and spiral ganglia, which is proposedly related to protection against subsequent traumatic noise exposure due to increased Ca^{2+} buffering capacity [21].

Taken together, we suggest that the lack of a neuroprotective protein calretinin in the modiolar-side fibers might be associated with vulnerability to noise-induced trauma.

ACKNOWLEDGEMENTS

This work was supported by the Research fund of Samsung Medical Center (EY, 2015-2017), and the Korea Health Technology R&D Project through the Korea Health Industry Development Institute (KHIDI), funded by the Ministry of Health & Welfare, Republic of Korea (grant number: HI17C0952).

The authors thank Dr. Sung Hwa Hong for his critical comments and financial support.

Author contributions: KS and EY conceived the idea, designed the experiments, and wrote the initial draft. KS, YS, and EY performed the experiments, analyzed the data, and wrote the manuscript.

REFERENCES

1. Berglund AM, Ryugo DK (1987) Hair cell innervation by spiral ganglion neurons in the mouse. J Comp Neurol 255:560-570.
2. Stamataki S, Francis HW, Lehar M, May BJ, Ryugo DK (2006) Synaptic alterations at inner hair cells precede spiral ganglion cell loss in aging C57BL/6J mice. Hear Res 221:104-118.
3. Liberman MC, Dodds LW, Pierce S (1990) Afferent and efferent innervation of the cat cochlea: quantitative analysis with light and electron microscopy. J Comp Neurol 301:443-460.
4. Taberner AM, Liberman MC (2005) Response properties of single auditory nerve fibers in the mouse. J Neurophysiol 93:557-569.
5. Liberman MC (1982) Single-neuron labeling in the cat auditory nerve. Science 216:1239-1241.
6. Furman AC, Kujawa SG, Liberman MC (2013) Noise-induced cochlear neuropathy is selective for fibers with low

spontaneous rates. J Neurophysiol 110:577-586.
7. Liberman LD, Wang H, Liberman MC (2011) Opposing gradients of ribbon size and AMPA receptor expression underlie sensitivity differences among cochlear-nerve/hair-cell synapses. J Neurosci 31:801-808.
8. Merchan-Perez A, Liberman MC (1996) Ultrastructural differences among afferent synapses on cochlear hair cells: correlations with spontaneous discharge rate. J Comp Neurol 371:208-221.
9. Kantardzhieva A, Liberman MC, Sewell WF (2013) Quantitative analysis of ribbons, vesicles, and cisterns at the cat inner hair cell synapse: correlations with spontaneous rate. J Comp Neurol 521:3260-3271.
10. Furness DN, Lawton DM (2003) Comparative distribution of glutamate transporters and receptors in relation to afferent innervation density in the mammalian cochlea. J Neurosci 23:11296-11304.
11. D'Orlando C, Celio MR, Schwaller B (2002) Calretinin and calbindin D-28k, but not parvalbumin protect against glutamate-induced delayed excitotoxicity in transfected N18-RE 105 neuroblastoma-retina hybrid cells. Brain Res 945:181-190.
12. Kalluri R, Monges-Hernandez M (2017) Spatial gradients in the size of inner hair cell ribbons emerge before the onset of hearing in rats. J Assoc Res Otolaryngol 18:399-413.
13. Dechesne CJ, Rabejac D, Desmadryl G (1994) Development of calretinin immunoreactivity in the mouse inner ear. J Comp Neurol 346:517-529.
14. Pyott SJ, Glowatzki E, Trimmer JS, Aldrich RW (2004) Extrasynaptic localization of inactivating calcium-activated potassium channels in mouse inner hair cells. J Neurosci 24:9469-9474.
15. Yi E, Roux I, Glowatzki E (2010) Dendritic HCN channels shape excitatory postsynaptic potentials at the inner hair cell afferent synapse in the mammalian cochlea. J Neurophysiol 103:2532-2543.
16. McLean WJ, Smith KA, Glowatzki E, Pyott SJ (2009) Distribution of the Na, K-ATPase alpha subunit in the rat spiral ganglion and organ of corti. J Assoc Res Otolaryngol 10:37-49.
17. Hackney CM, Mahendrasingam S, Penn A, Fettiplace R (2005) The concentrations of calcium buffering proteins in mammalian cochlear hair cells. J Neurosci 25:7867-7875.
18. Kujawa SG, Liberman MC (2009) Adding insult to injury: cochlear nerve degeneration after "temporary" noise-induced hearing loss. J Neurosci 29:14077-14085.
19. Liu W, Davis RL (2014) Calretinin and calbindin distribution patterns specify subpopulations of type I and type II spiral ganglion neurons in postnatal murine cochlea. J Comp Neurol 522:2299-2318.
20. Pangršič T, Gabrielaitis M, Michanski S, Schwaller B, Wolf F, Strenzke N, Moser T (2015) EF-hand protein Ca^{2+} buffers regulate Ca^{2+} influx and exocytosis in sensory hair cells. Proc Natl Acad Sci U S A 112:E1028-E1037.
21. Alvarado JC, Fuentes-Santamaría V, Gabaldón-Ull MC, Jareño-Flores T, Miller JM, Juiz JM (2016) Noise-induced "toughening" effect in wistar rats: enhanced auditory brainstem responses are related to calretinin and nitric oxide synthase upregulation. Front Neuroanat 10:19.
22. Nemzou N RM, Bulankina AV, Khimich D, Giese A, Moser T (2006) Synaptic organization in cochlear inner hair cells deficient for the CaV1.3 (alpha1D) subunit of L-type Ca^{2+} channels. Neuroscience 141:1849-1860.
23. Buckiová D, Syka J (2009) Calbindin and S100 protein expression in the developing inner ear in mice. J Comp Neurol 513:469-482.
24. Coate TM, Spita NA, Zhang KD, Isgrig KT, Kelley MW (2015) Neuropilin-2/Semaphorin-3F-mediated repulsion promotes inner hair cell innervation by spiral ganglion neurons. Elife 4:e07830.
25. Barclay M, Ryan AF, Housley GD (2011) Type I vs type II spiral ganglion neurons exhibit differential survival and neuritogenesis during cochlear development. Neural Dev 6:33.
26. Kim KX, Rutherford MA (2016) Maturation of NaV and KV channel topographies in the auditory nerve spike initiator before and after developmental onset of hearing function. J Neurosci 36:2111-2118.
27. Coate TM, Raft S, Zhao X, Ryan AK, Crenshaw EB 3rd, Kelley MW (2012) Otic mesenchyme cells regulate spiral ganglion axon fasciculation through a Pou3f4/EphA4 signaling pathway. Neuron 73:49-63.
28. Wang SZ, Ibrahim LA, Kim YJ, Gibson DA, Leung HC, Yuan W, Zhang KK, Tao HW, Ma L, Zhang LI (2013) Slit/Robo signaling mediates spatial positioning of spiral ganglion neurons during development of cochlear innervation. J Neurosci 33:12242-12254.
29. Delacroix L, Malgrange B (2015) Cochlear afferent innervation development. Hear Res 330:157-169.
30. Whitlon DS, Zhang X, Kusakabe M (1999) Tenascin-C in the cochlea of the developing mouse. J Comp Neurol 406:361-374.
31. Simonneau L, Gallego M, Pujol R (2003) Comparative expression patterns of T-, N-, E-cadherins, beta-catenin, and polysialic acid neural cell adhesion molecule in rat cochlea

during development: implications for the nature of Kölliker's organ. J Comp Neurol 459:113-126.
32. Druckenbrod NR, Goodrich LV (2015) Sequential retraction segregates SGN processes during target selection in the cochlea. J Neurosci 35:16221-16235.
33. Wu JS, Young ED, Glowatzki E (2016) Maturation of spontaneous firing properties after hearing onset in rat auditory nerve fibers: spontaneous rates, refractoriness, and interfiber correlations. J Neurosci 36:10584-10597.
34. Liberman LD, Liberman MC (2016) Postnatal maturation of auditory-nerve heterogeneity, as seen in spatial gradients of synapse morphology in the inner hair cell area. Hear Res 339:12-22.
35. Johnson SL, Marcotti W, Kros CJ (2005) Increase in efficiency and reduction in Ca2+ dependence of exocytosis during development of mouse inner hair cells. J Physiol 563:177-191.
36. Wong AB, Jing Z, Rutherford MA, Frank T, Strenzke N, Moser T (2013) Concurrent maturation of inner hair cell synaptic Ca^{2+} influx and auditory nerve spontaneous activity around hearing onset in mice. J Neurosci 33:10661-10666.
37. Ohn TL, Rutherford MA, Jing Z, Jung S, Duque-Afonso CJ, Hoch G, Picher MM, Scharinger A, Strenzke N, Moser T (2016) Hair cells use active zones with different voltage dependence of Ca^{2+} influx to decompose sounds into complementary neural codes. Proc Natl Acad Sci U S A 113:E4716-E4725.
38. Lin HW, Furman AC, Kujawa SG, Liberman MC (2011) Primary neural degeneration in the guinea pig cochlea after reversible noise-induced threshold shift. J Assoc Res Otolaryngol 12:605-616.
39. Ruel J, Bobbin RP, Vidal D, Pujol R, Puel JL (2000) The selective AMPA receptor antagonist GYKI 53784 blocks action potential generation and excitotoxicity in the guinea pig cochlea. Neuropharmacology 39:1959-1973.
40. Schwaller B (2014) Calretinin: from a "simple" Ca^{2+} buffer to a multifunctional protein implicated in many biological processes. Front Neuroanat 8:3.
41. Schwaller B (2010) Cytosolic Ca^{2+} buffers. Cold Spring Harb Perspect Biol 2:a004051.
42. Lukas W, Jones KA (1994) Cortical neurons containing calretinin are selectively resistant to calcium overload and excitotoxicity in vitro. Neuroscience 61:307-316.
43. Kotti T, Tapiola T, Riekkinen PJ Sr, Miettinen R (1996) The calretinin-containing mossy cells survive excitotoxic insult in the gerbil dentate gyrus. Comparison of excitotoxicity-induced neuropathological changes in the gerbil and rat. Eur J Neurosci 8:2371-2378.
44. Todkar K, Scotti AL, Schwaller B (2012) Absence of the calcium-binding protein calretinin, not of calbindin D-28k, causes a permanent impairment of murine adult hippocampal neurogenesis. Front Mol Neurosci 5:56.
45. Caicedo A, d'Aldin C, Eybalin M, Puel JL (1997) Temporary sensory deprivation changes calcium-binding proteins levels in the auditory brainstem. J Comp Neurol 378:1-15.
46. Fuentes-Santamaria V, Alvarado JC, Taylor AR, Brunso-Bechtold JK, Henkel CK (2005) Quantitative changes in calretinin immunostaining in the cochlear nuclei after unilateral cochlear removal in young ferrets. J Comp Neurol 483:458-475.
47. Li J, Zhou X, Huang L, Fu X, Liu J, Zhang X, Sun Y, Zuo M (2013) Alteration of CaBP expression pattern in the nucleus magnocellularis following unilateral cochlear ablation in adult zebra finches. PLoS One 8:e79297.